Neuron
Article

A Synaptic Strategy for Consolidation of Convergent Visuotopic Maps

Marnie A. Phillips,[1,2,*] Matthew T. Colonnese,[5] Julie Goldberg,[2] Laura D. Lewis,[2] Emery N. Brown,[2,4,6] and Martha Constantine-Paton[1,2,3]
[1]McGovern Institute for Brain Research
[2]Department of Brain and Cognitive Sciences
[3]Department of Biology
[4]MIT-Harvard Division of Health Sciences and Technology
Massachusetts Institute of Technology, Cambridge, MA 02139, USA
[5]INSERM, U901, INMED, Aix-Marseille Université, Faculté des Sciences, 13273 Marseille, France
[6]Neuroscience Statistics Research Laboratory, Department of Anesthesia, Critical Care, and Pain Medicine, Massachusetts General Hospital, Boston, MA 02114, USA
*Correspondence: marnie.a.phillips@gmail.com
DOI 10.1016/j.neuron.2011.06.023

SUMMARY

The mechanisms by which experience guides refinement of converging afferent pathways are poorly understood. We describe a vision-driven refinement of corticocollicular inputs that determines the consolidation of retinal and visual cortical (VC) synapses on individual neurons in the superficial superior colliculus (sSC). Highly refined corticocollicular terminals form 1–2 days after eye-opening (EO), accompanied by VC-dependent filopodia sprouting on proximal dendrites, and PSD-95 and VC-dependent quadrupling of functional synapses. Delayed EO eliminates synapses, corticocollicular terminals, and spines on VC-recipient dendrites. Awake recordings after EO show that VC and retina cooperate to activate sSC neurons, and VC light responses precede sSC responses within intervals promoting potentiation. Eyelid closure is associated with more protracted cortical visual responses, causing the majority of VC spikes to follow those of the colliculus. These data implicate spike-timing plasticity as a mechanism for cortical input survival, and support a cooperative strategy for retinal and cortical coinnervation of the sSC.

INTRODUCTION

Eye-opening (EO) in rodents, or birth in humans, marks the onset of an eventful period in visual development. By the time of EO, cortical response properties are newly prepared to process high frequency pattern stimuli (Colonnese et al., 2010). After this point, high quality visual experience is critical for the refinement of receptive fields and response properties in visual areas, and normal vision in the adult (Maffei et al., 2004; Maurer et al., 2005; Ostrovsky et al., 2006; Smith and Trachtenberg, 2007; White et al., 2001; Yu et al., 2010). In rodents the onset of visual experience at EO induces rapid (4–24 hr) physiological and biochemical effects in the superficial visual layer of the superior colliculus (sSC). These include delivery of the scaffold protein PSD-95 to spines and synaptic fractions (Yoshii et al., 2003), and transient increases in silent synapses containing the NR2B N-methyl-D-aspartate (NMDA) receptor subunit, functional synapse maturation, and input refinement (Lu and Constantine-Paton, 2004).

EO-triggered changes occur during the major period of synaptogenesis in the rodent sSC (Bakkum et al., 1991; Lund and Lund, 1971; Warton and McCart, 1989), where two primary glutamatergic visual pathways converge. Retinal axons arrive in the sSC embryonically and their terminal arbors are restricted to topographically appropriate zones as early as P4, and refined at least 1 day before EO (Dhande et al., 2011; Simon and O'Leary, 1992). The refinement of the projection from visual cortex (VC) is delayed. Visual cortical axons from layer 5 do not arrive in mouse sSC until postnatal day (P) 4 (Inoue et al., 1992; Thong and Dreher, 1986), and only by P12, just before EO, do their arbors occupy roughly retinotopically appropriate regions (Triplett et al., 2009).

Much recent work in rodents has documented the role of activity in the emergence of mapped visual projections. Visuotopic axon maps in the SC are initially roughly aligned using adhesion, repulsion, and early waves of synchronized retinal activity (Flanagan, 2006; Huberman et al., 2008a; Triplett et al., 2009). However, this topographic axon targeting precedes the major periods of synapse formation, functional maturation, and input refinement that coincide with the onset of environmental drive (Lu and Constantine-Paton, 2004). This "consolidation" phase of refinement in the sSC is likely to involve both synaptic elaboration and elimination as individual retinal and cortical axons sort their terminals on postsynaptic cells. Little is known about this process or its cellular mechanisms, which allow precise refinement of converging projections. Simple Hebbian mechanisms are predicted to suppress the later-arriving cortical inputs unless their activity is closely synchronized with that of earlier synapses (Constantine-Paton et al., 1990). This has led us to the hypothesis that late arriving, broadly mapped, inputs such as those from VC have specific adaptations to enable successful wiring.

Here we control EO to precisely define the onset of pattern vision, and combine this with in vivo anterograde labeling of retinal and cortical afferents to sSC and anatomical reconstruction of cells expressing a genetically encoded eGFP in a population of collicular neurons located at the interface of the two projections. We follow changes in these neurons and the cortical input in age-matched animals with opened or closed eyelids using quantitative structural and whole-cell patch clamp analyses. These approaches identify structural and functional changes at synapses over the EO interval of identified sSC neurons, and highlight those changes specifically controlled by early visual experience. In vivo multiunit recording of spontaneous and visually evoked activity in sSC and VC layer 5 of intact awake pups are used to reveal the relative latencies of vision-driven activity in cortex and sSC. These data provide evidence for a spike-timing dependent mechanism that underlies the successful stabilization of cortical synapses on sSC neurons with EO, and the net synaptic loss observed when the eyes remain closed.

RESULTS

A Role for EO-Induced Redistribution of the Postsynaptic Density Scaffold PSD-95 in Collicular Synaptogenesis

In this study, we focus on a distinct population of sSC neurons with vertically distributed and predominantly dorsal dendrites (dorsally oriented vertical [DOV] neurons) lying within both retinal and cortical terminal zones. These cells were labeled early in eGFP mice and are also identifiable with IR-DIC optics using laminar position, somatic shape, and dendritic orientation (Tokunaga and Otani, 1976).

Based on earlier work (Lu and Constantine-Paton, 2004; Philpot et al., 2001; Yoshii et al., 2003), and the finding that normal levels of PSD-95 are required to produce NMDA receptor-dependent long-term potentiation and depression (Béïque and Andrade, 2003; Migaud et al., 1998), we hypothesized that PSD-95 is crucial to rapid, EO-induced synaptic remodeling through its stabilization of synapses sensitive to the new stimuli. PSD-95 is highly expressed in DOV neurons and sSC synapses (see Figure S1 available online). In order to understand the mechanism by which cortex innervates the sSC, we first assayed EO-dependent synaptic development in the mouse sSC and then validated the PSD-95 hypothesis using DOV neurons from PSD-95 mutant mice.

Miniature excitatory postsynaptic currents (mEPSCs) were recorded from DOV neurons in acute sSC slices 1–2 days before EO (BEO), 1–2 days after EO (AEO), in age-matched animals whose eyes were never opened (EC), and after EO in PSD-95 mutant mice lacking this scaffold at the synapse (Figures 1A–1C and Figure S1). EO (or dark-rearing) in rodents has no effect on presynaptic release probability in lateral geniculate nucleus neurons or sSC (Chen and Regehr, 2000; Lu and Constantine-Paton, 2004), thus mEPSC event frequency over this interval was used to assay the relative abundance of release sites. Changes in mEPSC frequency and amplitude were measured using model-based analysis (Supplemental Experimental Procedures), an approach designed to accurately take into account the statistical distribution of synaptic current parameters within individual cells when calculating differences between groups. With this procedure significant differences between groups at $\alpha = 0.05$ are shown by the presence of non-overlapping 95% confidence intervals. Histograms in Figures 1D and 1E show distributions of mean frequency and amplitude of mEPSCs in each treatment group obtained after sampling each modeled distribution with a parametric bootstrap 500 times (samples).

To best assay functional synaptic development across the neuronal arbor, and avoid bias associated with analyzing only release sites likely to be located on thick dendrites or more proximal to the soma (Magee and Cook, 2000; Smith et al., 2003), we examined all suprathreshold events >11 pA without selecting events based on rise-time. Few synaptic events were observed BEO, but mean total mEPSC frequency in DOV cells increased significantly, on average 4-fold, AEO (Figure 1D). In the first 1–2 days AEO there was also a small increase in strength ~20% from BEO (Figure 1E). The small (3 pA) increase in mean amplitude observed could contribute to some of the new suprathreshold events detected AEO, however, it is not sufficient to account for these results. An average increase of 8 pA in the amplitude of these events would have been required to cause the 4-fold increase in frequency actually observed (Figure S1).

When eye closure was maintained (EC) past the normal EO day, the overall frequency of mEPSCs was reduced below pre-EO levels (Figure 1D), suggesting a net loss of synapses caused by obscured vision. The remaining synapses were also weakened, but were not significantly different from amplitudes before EO (Figure 1E).

EO induces translocation of PSD-95 to sSC synapses in rats, suggesting a role for this protein in synapse plasticity AEO. We confirmed the absence of PSD-95 from sSC synapses and DOV neurons in PSD-95 mutant mice (Figure S1). PSD-95 mutant animals with 1–2 days of visual experience AEO resembled pre-EO animals in terms of mEPSC frequency, confirming a role for this molecule in pattern vision induced synaptic increases. (Figure 1D). However, mEPSC amplitudes of the remaining synapses were normal in these mice (Figure 1E). These data suggest that PSD-95 is important for new synapse formation after EO, but in the absence of PSD-95, remaining synapses are still able to add glutamate receptors and be potentiated.

Distribution of Retinal and Cortical Afferents on DOV Neuronal Dendrites with Eye Opening

To identify the dendritic location of the EO-dependent synaptic plasticity, we examined the pattern of retinal and cortical afferent arborization on the dendrites of DOV neurons by anterograde labeling of retinal and VC afferents in eGFP mice at P29-30 when the number of high expressing cells was greatest (Figure 2A and Figure S2). VC axons were most dense in the deeper portion of the sSC, whereas contralateral retinal axons preferentially occupied more superficial positions (Figures 2B–2D). All eGFP-labeled DOV neurons were reproducibly located in the transition zone between the two projections, and electrical stimulation of retinal and cortical axons where they enter together in the brachium of the sSC could evoke unitary postsynaptic responses in these neurons (data not shown).

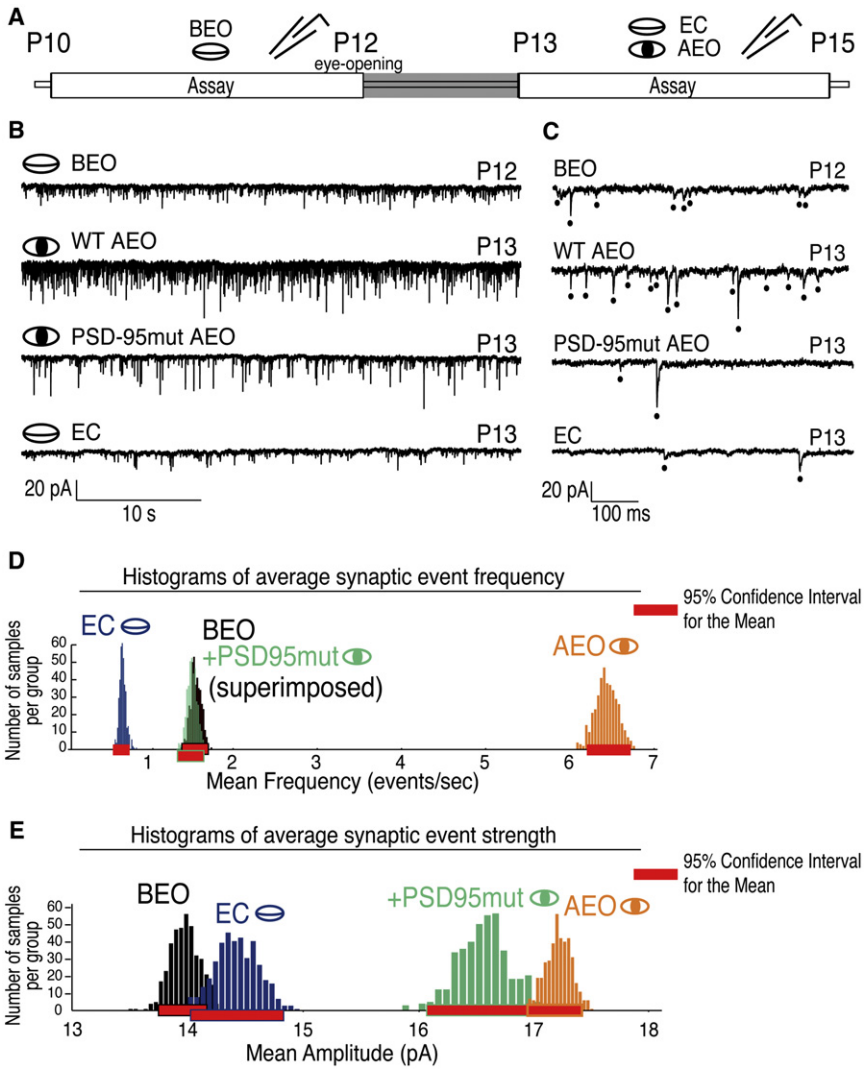

Figure 1. Vision Initiates Synaptogenesis in the Retino- and Cortico-Recipient sSC Requiring PSD-95

(A) Timeline.

(B) Examples of EO and PSD-95 dependent increases in frequency of mEPSCs in sSC dorsal-oriented vertical (DOV) neurons. Data is from before EO (BEO), after EO with normal levels of PSD-95 in wild-type mice (WT AEO), after EO in mutants lacking PSD-95 (PSD-95mut AEO), or cells from age-matched wild-type mice with the eyes kept closed (EC).

(C) Traces from (B) at expanded scale. Dots mark selected events.

(D) Parametric bootstrap-derived histograms show frequency for each experimental group with associated 95% confidence interval (bar at base of distribution). Mean frequency increased approximately 4-fold AEO and requires PSD-95. Prevention of EO reduces miniature currents below pre EO levels. (BEO, n = 6; PSD-95$^{-/-}$ AEO, n = 3; EC, n = 4, WT AEO, n = 6.)

(E) Amplitudes for remaining synapses in the PSD-95 mutant are not significantly different from WT cells AEO. Amplitudes for the BEO and EC animals are reduced relative to the EO groups.

We identified the potential locus of contact of retinal and cortical axons onto these neurons, by analyzing the colocalization of each afferent population and the eGFP-labeled dendritic arbor (Figures 2E–2G). The degree of chance overlap was estimated by rotation of the images containing the particular afferent label 90° in the plane of section with respect to the images containing the GFP label (Supplemental Experimental Procedures). The mean size and number of overlapped pixel clusters in rotated images was significantly smaller than control images. This is demonstrated in Figure 2E (arrowhead), where a portion of a labeled retinal axon is observed to course alongside a length of eGFP dendrite.

DOV dendrites are highly branched with a variable dendritic branching structure and did not conform to standard definitions of secondary or tertiary branches used in traditional classification schemes for pyramidal neurons. To examine the relationship of these afferent projections to dendritic structure we subdivided the arbor regions by caliber at each branch point with successively thinner segments ranked from 1 to 4. Three-dimensional neurolucida reconstructions of two neurons, including the labeled neuron in Figure 2, illustrate the distribution of ranked segments (Figure 2H) (see Supplemental Experimental Procedures for classification details).

Dendrite caliber rank is a significant factor affecting the distribution of potential contact points for both retinal (F statistic = 11.58, $n = 43$, $p < 0.05$) and cortical ($F = 3.57$, $n = 37$, $p < 0.0001$) axons (Figure 2I, significance between calibers assessed with Games-Howell post hoc). Thus, although DOV neurons are apposed to both retinal and visual cortical afferents, after EO retinal axons dominate dendrites that are thin and generally distal (caliber 4), and cortical afferents are most frequently apposed to dendrites of medium thickness, generally proximal (caliber 3). This raised questions about the relative positions of these two inputs just before EO. The overall "opposing gradient" pattern of innervation was also observed before EO (Figures 3A–3G). Of the 124 Thy1 eGFP pups with both retina and cortical labeling surgeries on P9, both inputs were successfully labeled on only one P11 DOV neuron with sufficient dendritic labeling to unambiguously identify it as a DOV neuron. We found retinal axons in close contact with the proximal dendrites and dorsal somata of this neuron, whereas cortical axons were mostly restricted to the ventral portion of the soma (Figures 3F and 3G). This apparent difference in location of the cortical and retinal axons before and after EO in young adults suggests that cortical inputs move to dendrites and displace existing retinal terminals to more distal dendritic sites during high quality pattern vision. In

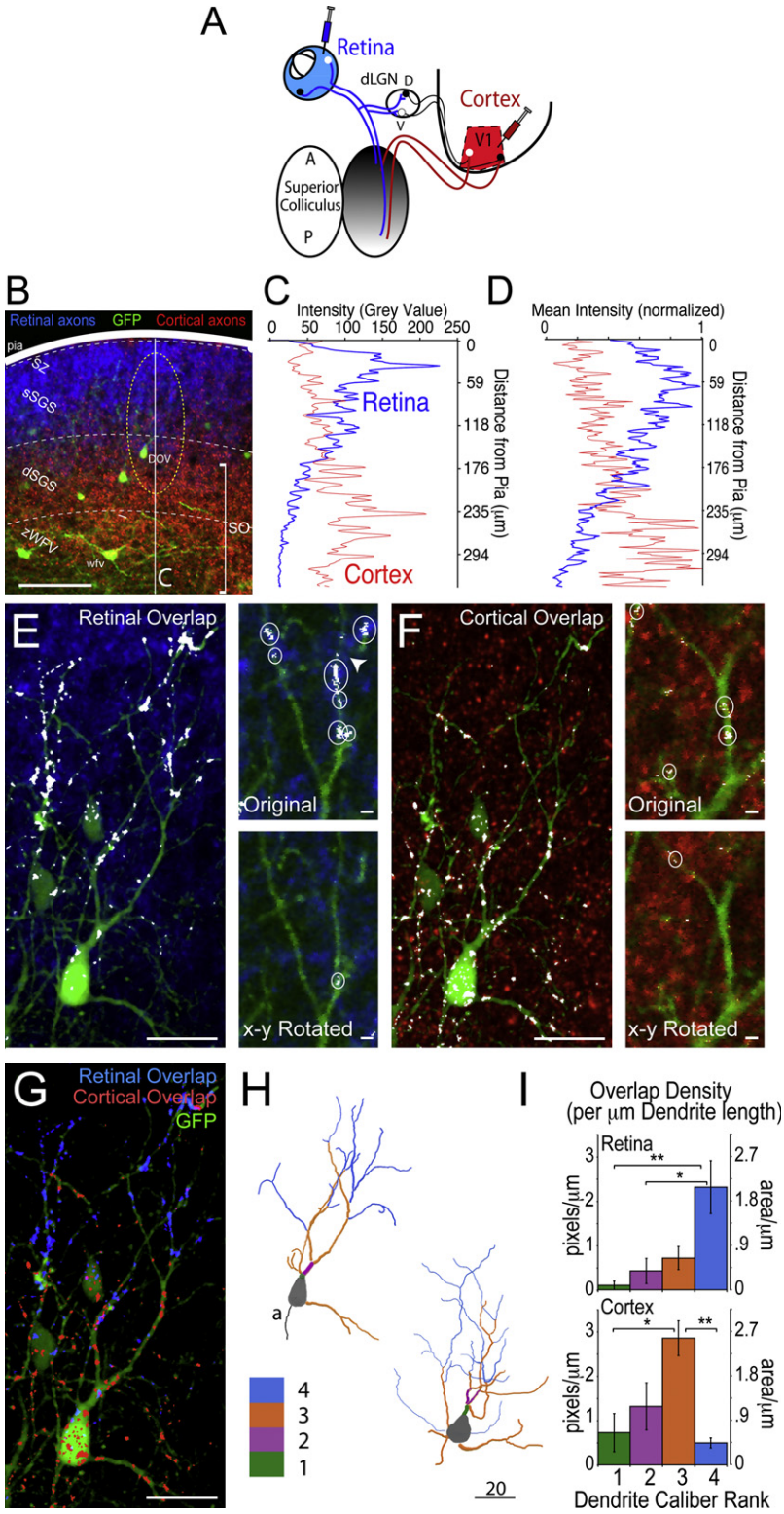

Figure 2. Sorting of Cortical and Retinal Axons on the Dendritic Arbor of DOV Neurons after EO (P29–30)

(A) Diagram of dual color anterograde tract tracing in eGFP mice.

(B) Representative eGFP-expressing DOV cell after labeling of axons from retina and visual cortex. DOV neurons (circled) are located in the deep portion of the stratum griseum superficiale (dSGS) at the interface of retinal and cortical afferents. Pial membrane fluorescence is removed. SZ = stratum zonale, sSGS = superficial stratum of SGS, zWFV = zone of wide-field vertical neurons, SO = stratum opticum. Scale bar, 100 μm.

(C) Pixel intensity profiles along the solid white line in (B).

(D) Mean pixel intensity profiles for the contralateral retina and ipsilateral cortex (n = 3 animals).

(E) Confocal projection showing overlapped pixels (white) between retinal axons (blue) and eGFP (green). Scale bar, 20 μm. Adjacent are magnified comparisons of original images and rotated controls to detect nonspecific overlap of retinal axons (Supplemental Experimental Procedures). Scale bar, 2 μm.

(F) Same as (E) for cortical axons.

(G) Distribution of the overlapped pixels, on the same neuron from either the retinal (blue) or cortical (red) projection. Scale bar, 10 μm.

(H) Neurolucida reconstructions of two DOV dendritic arbors, including the cell in (E) (upper). Dendritic segments were categorized according to their average thickness between branch points (Supplemental Experimental Procedures).

(I) Quantification of the distribution of overlapped retinal or cortical pixels per μm of caliber-identified dendritic segment, measured in confocal z series from three reconstructed neurons. Equivalent overlap area in micronsμm per micronof dendritic length, on right axis. *$p < 0.05$, **$p < 0.01$, Games-Howell post hoc.

support of such invasive ability, it is only after EO that corticocollicular inputs become the primary inhibitor of dorsally directed sprouting of the ipsilateral retinal projection following an early contralateral retinal lesion (Colonnese and Constantine-Paton, 2001).

Synaptic Development in DOV Neurons Involves a Transient Sprouting of Filopodia over EO

GFP-labeled DOV neurons at P13, 1 day after EO, have abundant dendritic protrusions and appear "hairy" (Figures 4A–4D). Densities of spines and filopodia were examined across the dendritic arbor of developing DOV neurons, with dendrites classed by caliber rank. Filopodia (length > 3 width) have been characterized as new or particularly dynamic protrusions, whereas spines (length $\leq$ 3 width) are more likely to contain matured, stronger, or stabilized synapses (see Supplemental Experimental Procedures). These criteria were used to quantify structural changes indicative of synaptogenesis on dually innervated DOV neurons before (P11) and 24 hr after controlled EO (P13) as well as 4 days AEO (P16) and at least 20 days AEO (adult) (Figures 4E and 4F).

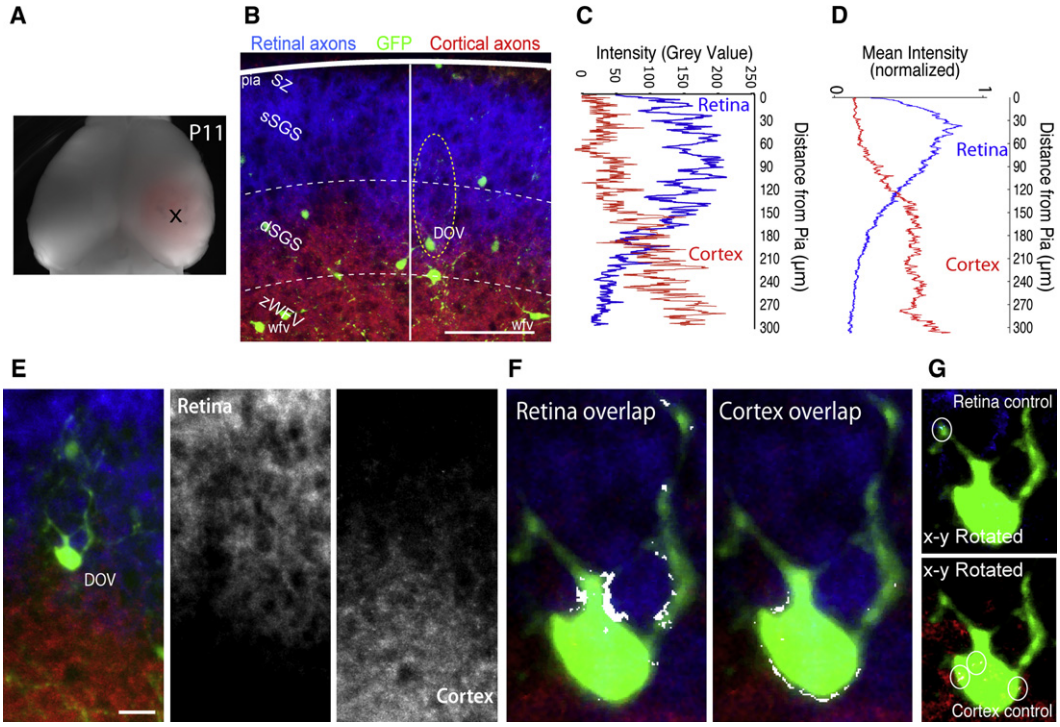

Figure 3. Retinal and Visual Cortical Inputs to sSC before EO

(A) Cortical label extent confirmed at sacrifice on P11.

(B) eGFP-expressing DOV neuron after dual labeling of axons from retina and VC.

(C) Pixel intensity profiles along the solid white line in (B) show opposing distributions of retinal and cortical label at increasing depth from pia at P11.

(D) Mean pixel intensity profiles for the contralateral retina and ipsilateral cortex (n = 5 animals).

(E) Confocal projection showing a DOV neuron at the interface of the contralateral retinal input (blue) and the ipsilateral cortex (red). Scale bar, 10 μm.

(F) Confocal optical slice showing overlapped pixels (white) between retinal axons (blue) and eGFP (green). Proximal dendritic sites overlap with retinal axons and cortical axons are apposed to somatic sites. Scale bar, 10 μm.

(G) Rotated control images used to detect nonspecific overlap of retinal and cortical axons. Some overlap is still detected, but these clusters are few (circled), and smaller in size.

Dendrites of all calibers had few filopodia at P11, but rapidly developed a high density of filopodia by P13 that were eliminated by P16 (Figure 4F). These changes reached significance on the thinnest and most abundant dendrites, caliber 3 and caliber 4. Significant changes in spine density were not observed with age (one-way ANOVA, $p > 0.05$, calibers 2, 3, 4). Between the youngest and oldest ages studied (P11 and "Adult"), there were detectable but small mean increases in both total dendritic branch length and the complexity of arbors (Figure S3). Small increases in apical dendritic complexity and length occurred proximal, but not distal, to the soma, suggesting that maturing cells added new synaptic space proximally.

Prevention of Eye Opening Eliminates Spines on Cortex-Targeted Dendritic Segments

We tested whether the surge in filopodia at EO required visual experience by comparing P13 littermates whose eyes were opened (EO) or closed (EC) (Figure 5A). Prevention of EO allows diffuse light to pass through eyelids but blocks high contrast vision (Krug et al., 2001). EC did not prevent filopodial sprouting. Instead it resulted in a specific reduction of spine density on the caliber 3 dendrites normally dominated by VC after EO (Figures 5B and 5C). Spines and filopodia on caliber 4 dendrites were unaffected ($n = 25$, $p > 0.50$).

These results suggest a two-step process driving dendritic development at EO: a pattern vision independent induction of filopodia and a pattern-vision dependent spine retention on VC-recipient dendrites.

Pattern-Vision Dependent Refinement of Corticocollicular Axon Terminals

The changes described above suggest a particular role for EO in sprouting and synapse formation by VC afferents. To examine this, we labeled small numbers of corticocollicular axons in rat pups (their larger size compared to mice making specific labeling of a smaller subset of cortical neurons possible). Single strands of DiI-saturated Gelfoam were inserted in the monocular, medial region of ipsilateral VC (Figure 5D), a region that projects to posterior-dorsal sSC and responds to the same visual field locale as retinocollicular axons terminating in that region (Khachab and Bruce, 1999). Maximal DiI spread from the center of these topographic injections extended on average 9.2% of the anterior-posterior (A-P) axis of the cortex, and never >12.5%. Reconstructions of corticocollicular axons illustrate that at

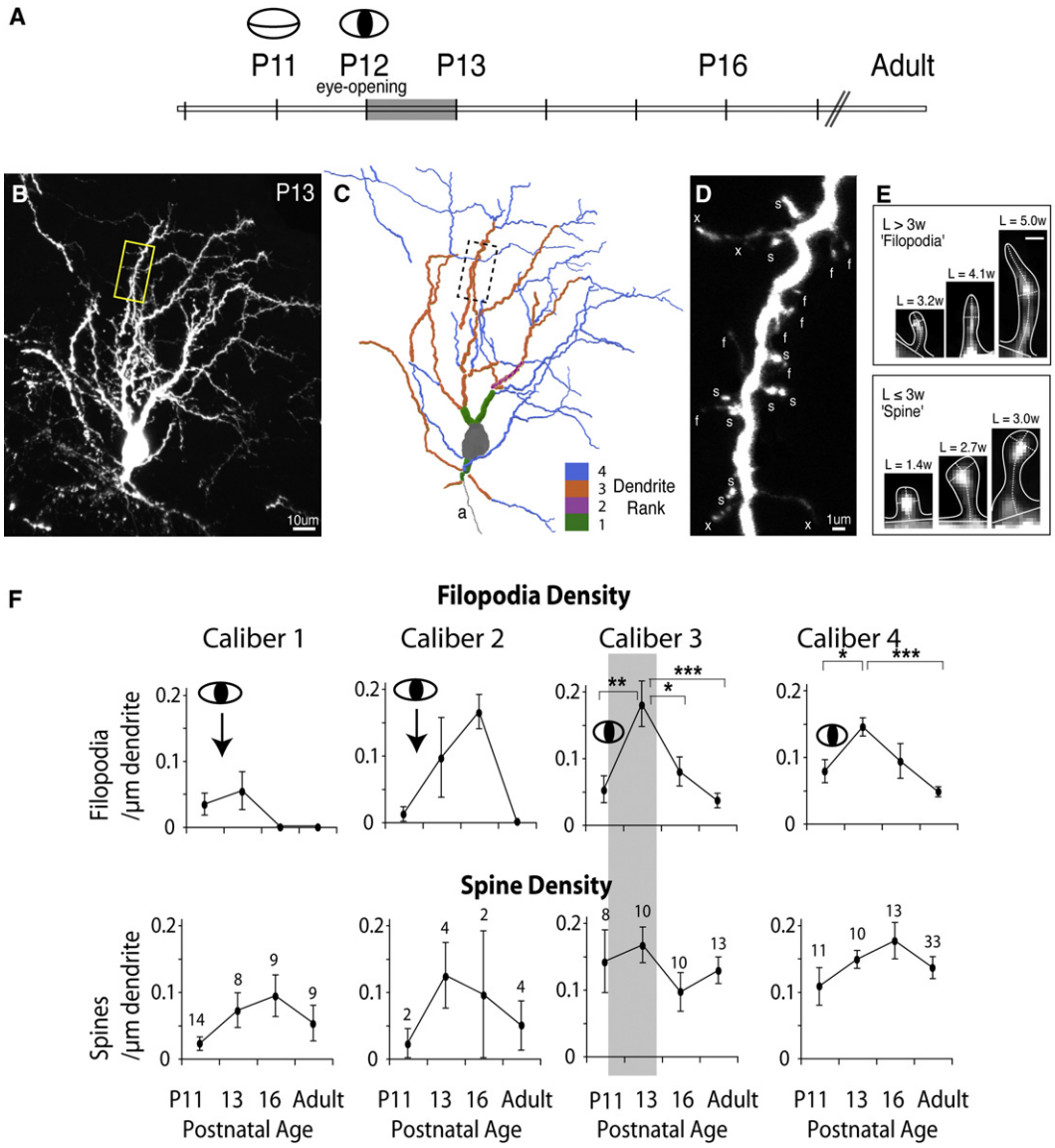

Figure 4. A Transient Developmental Surge in Filopodia after EO

(A) Timeline. EO = P12–P13. DOV dendrites were analyzed before EO (P11–P12), 1 day after EO (P13), 4 days after EO (P16), or after P30 (Adult).

(B) Z series projection of an eGFP labeled DOV neuron at P13 with the typical "hairy" appearance observed after EO. Scale bar, 10 µm.

(C) Neurolucida reconstruction of the boxed region in (B). Dendritic segments are categorized according to their caliber rank as measured from original images.

(D) Enlargement of boxed region in (B). Protrusions were classified at high magnification as "filopodia" (f) or "spines" (s) as described in (E). Long protrusions much longer than 6 times their width were not counted (x). Scale bar, 1 µm.

(E) Classification as "Spine" or "Filopodia" according to the length versus maximal width ratio at threshold shown. L = 3D length from base to tip. w = width at widest point (neck or head). Protrusions < 0.6 µm long were not counted. Scale bar, 0.5 µm.

(F) Quantification of filopodia increases over EO on caliber 3 (6–13 cells at each age, $^{**}p < 0.01$, Tukey HSD post hoc) and caliber 4 ($^{*}p < 0.05$) that return to baseline at P16 on caliber 3 ($^{*}p < 0.05$), and by adulthood on caliber 4 ($^{***}p < 0.001$). No significant increase in spines was detected over EO ($p > 0.05$, Tukey HSD post hoc). Dendritic segments analyzed at each age are given in the spine plots. Caliber 2 branches were rare. No. of dendritic protrusions measured: n = 343 P11; n = 652 P13; n = 233 P16, n = 364 adult.

P12-P13, just before EO in rat, individual corticocollicular axon terminals extend ectopic side branches along their anterior-posterior (A-P) length before terminating in the posterior third of the sSC, where some tended to be more highly branched (BEO; Figure 5E). The collateral branching pattern was reminiscent of the early retinocollicular projection (Simon and O'Leary, 1992). By P15-P16, however, 2–3 days AEO on P13, ectopic side branches were reduced, whereas the terminal zone (TZ) arbor became densely branched.

To examine the pattern-vision dependence of the VC axonal sprouting/refinement, eyelids of littermates of the same animals were sutured closed on P13, before EO. Two to three days of eye

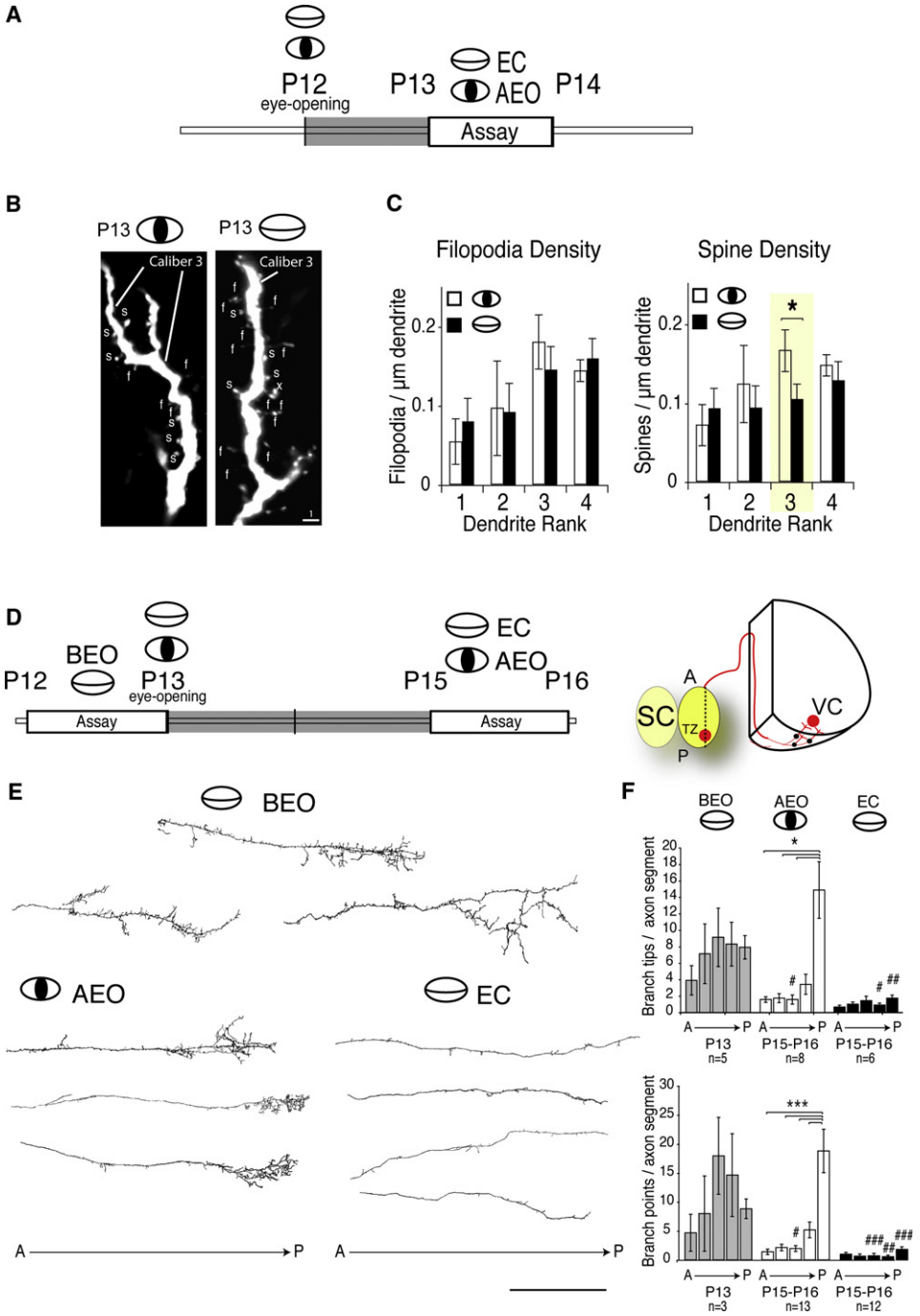

Figure 5. Eyelid Closure Eliminates Spines on VC-Recipient Dendrites and Strips Corticocollicular Axons of Their Terminal Zone Arbors

(A) Timeline. EO was on P12. DOV neurons in sSC were analyzed 1 day after EO (P13 EO) or in age-matched littermates with eyes closed over the same period (P13 EC).

(B) Representative confocal projections of caliber 3 dendrites with eyes opened or closed.

(C) Filopodial densities were unaffected by EO or EC, but EO was required to maintain spine densities on caliber 3 dendrites ($p < 0.05$ Student's t test with Bonferroni correction).

(D) Timeline for VC DiI labeling and analysis of EO versus EC effects on corticocollicular axons in rat pups at equivalent ages.

(E) Neurolucida reconstructions of corticocollicular axons before EO (BEO) and after EO at P15–P16 (AEO), or in the age-matched eye closed condition (EC). A = anterior; p = posterior. Scale bar, 250 µm.

(F) Quantification of age and EO-dependent changes in axon branching. (One-way ANOVA for effect of location $p < 0.05$; Tukey HSD post hoc test *$p < 0.05$, ***$p < 0.001$; two-tailed Student's t test for effect of treatment #$p < 0.05$, ##$p < 0.01$, ###$p < 0.001$ with Bonferroni correction.)

closure resulted in a dramatic change in corticocollicular terminals. The TZ normally seen after EO was not present, and only infrequent short collateral branches remained along the VC axon (EC; Figure 5E). This suggests robust pruning of VC synapses occurred in the visually deprived condition. To quantify these EO dependent changes, 160 mm^3 volumes of tissue were sampled at regular intervals along the A-P length of the sSC. The complexity of the VC arbors within these volumes was measured by counting branch points and end points on each segment of all cortically labeled axons. After EO, axons in the posterior fifth of the sSC had significantly more branch points and endpoints compared to the anterior sSC (Figure 5F). Eye-closed animals show no terminal complexity; all axons were significantly reduced along their collicular length in the number of branch and end points with respect to both after and before EO. These results show a requirement for pattern vision in the local refinement and maintenance of topographically appropriate corticocollicular arbors and probably also in the synapses they establish.

Visual Cortex Is Required for EO-Dependent Formation of Functional Contacts in sSC and an EO-Independent Induction of Filopodia at Proximal Sites

To test the dependence of collicular synaptogenesis specifically on the rapidly arborizing corticocollicular projection, we assayed the effect of removing the VC input before EO on spontaneous whole-cell mEPSCs and the locus of any changes in spine and filopodia distribution on DOV neurons.

Lesions of ipsilateral VC were made in eGFP transgenic mice between P9-P10 by microaspiration of the cellular layers of VC (Figure S4 and Supplemental Experimental Procedures). Animals received either a lesion that eliminated the collicular-projecting Layer V pyramidal cells (VC removed) or surgery with skull-flap incision but without cortical aspiration (sham) (Figure 6A).

Consistent with a loss of cortical synapse formation after VC lesion, removal of VC resulted in a significant reduction of mEPSC frequency (Figures 6B and 6C) after EO compared to sham-operated controls. The enhancement in mEPSC amplitude, however, represents a significant potentiation of the remaining largely retinal synapses compared to EO sham animals (Figure 6D). This increase in strength of remaining inputs after VC removal suggests a competition between retinal and cortical driven synapses during normal visual synaptogenesis.

No significant effect of VC removal was observed on filopodia or spine density on caliber 4 dendrites ($p > 0.70$, $n = 23$ lesion, $n = 24$ sham), consistent with the hypothesis that these dendrites contain primarily retinal inputs, whose strength (rather than number) was adjusted after VC lesion.

VC removal prevented the normal appearance of filopodia on caliber 3 dendrites but had no significant effect on spine density ($p > 0.90$, $n = 9$ lesion, $n = 9$ sham) (Figures 6E and 6F), suggesting that filopodia are the sites of new cortical synapse formation. Caliber 3 dendrites are predominantly localized in mid-stratum griseum superficiale (SGS) levels where cortical and retinal terminals overlap, and are the most likely to be contacted by cortical axons. Thus the presence of cortical afferents/growth cones in the neuropil appears necessary for the development of new functional contacts, and also triggers the formation of filopodia on caliber 3 dendrites, on which many of these new contacts form.

Visual Cortical Activity Facilitates Collicular Responses In Vivo 1–2 Days after EO

Hebbian theory suggests that the synaptic elaboration of the late-arriving visual cortical inputs should be at a significant competitive disadvantage compared to the previously established mapped retinal synapses. Nevertheless, cortex successfully establishes a synaptic foothold at proximal sites, in a vision-dependent manner. Such rapid expansion is an apparent violation of Hebb's postulate, unless the cortical activity does in fact precede and contribute to driving collicular responses. We examined this possibility by measuring visual responses in vivo simultaneously from the sSC projecting layer of VC (lower layer 5a) and the ipsilateral sSC of the same animals 1–2 days after EO. This is during the period of EO dependent plasticity in the rat sSC (Lu and Constantine-Paton, 2004) (Figure 7A). Because anesthesia at any level has significant effects on activity at this age (Colonnese et al., 2010), we used an awake, unanesthetized preparation.

Multiunit ON responses to whole-field light flash under ambient illumination in the VC layer 5a precede visual responses throughout the depth of the ipsilateral SC (Figure 7B and Supplemental Experimental Procedures). This was surprising, because retinal ganglion cells project directly to the sSC, compared to at least three synaptic delays in the retino-thalamo-cortical output pathway. Lower detection thresholds did not reveal any responses in the superficial SGS that preceded the cortical visual response, suggesting that we have not undersampled small superficial retino-recipient cells in our analysis (Figure S5). Latency of the ON response in layer 5a relative to the deep SGS (where DOV neurons are located) was approximately10 ms, and was specific for the ON response (Figure 7C). By contrast, OFF collicular responses were coincident with the cortex, perhaps a result of a strong input from an OFF ganglion cell class that projects specifically to the deep SGS (Huberman et al., 2008b). The short latency of collicular ON responses following cortical output suggests that after EO cortical activity is a strong driver of the deep SGS cells where DOV neurons are located. To test the contribution of cortex to this response, we suppressed cortical contributions to the visual response by induction of cortical spreading depression. We found that cortical suppression delayed and diminished collicular ON responses (Figure 7D). Visual responses in sSC were not entirely eliminated, however, suggesting that the remaining, sluggish response is retina driven. Thus, as early as 1–2 days after EO cortical input activity precedes the sSC response, and cooperates with retinal synapses to fire collicular neurons in deep SGS.

Network State Changes Linked to Eye Closure Delay Light Responses in VC Layer 5a

To identify the mechanism by which eye closure depresses synaptogenesis in the sSC, we directly measured the effect of eyelid closure on visual cortical activity in the young, awake pups (Figure 8A). As early as 1 day after normal EO, animals with closed eyelids displayed a change in activity state characterized by

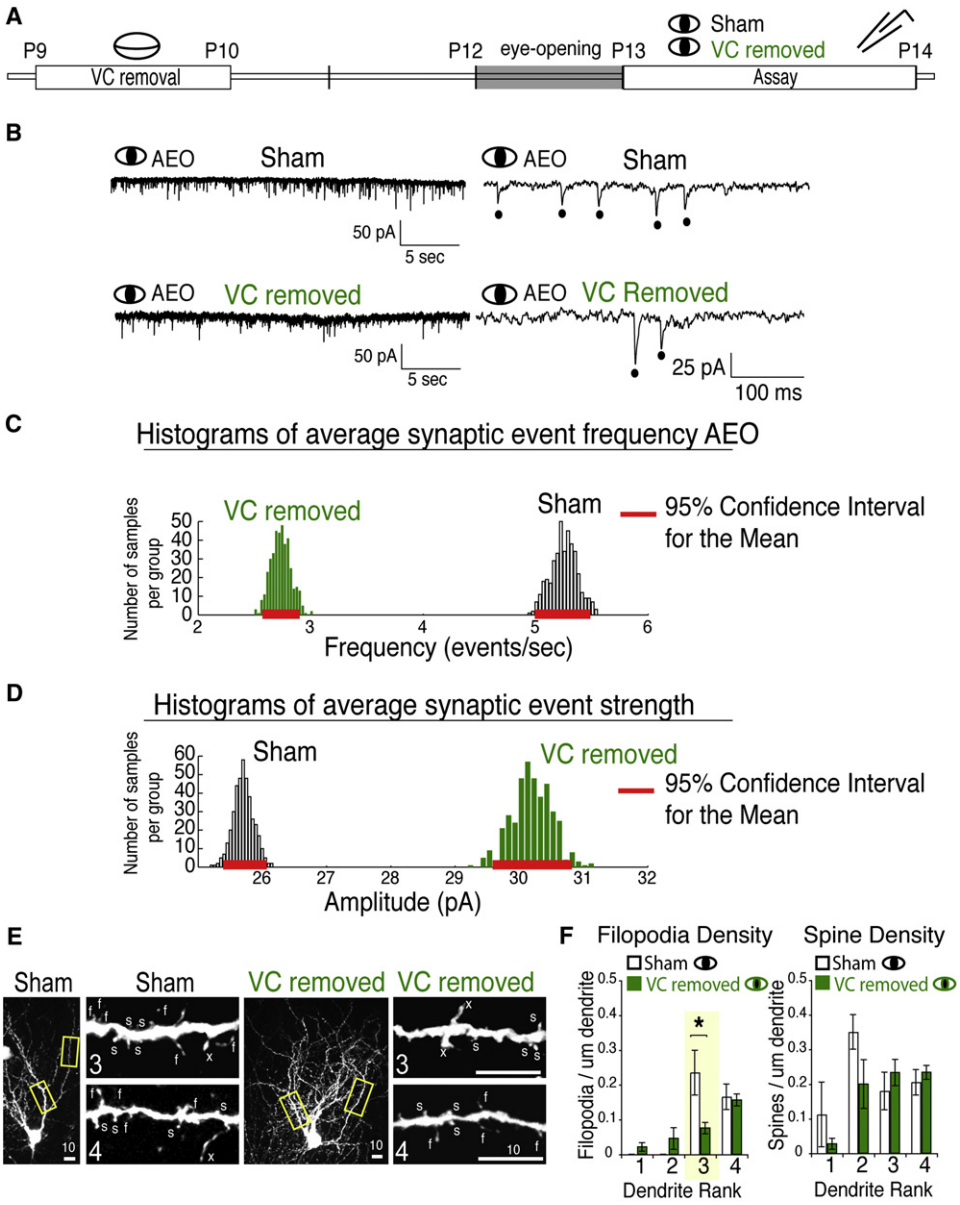

Figure 6. VC Axons Induce Filopodia Development and Are Required for Vision-Dependent Synaptic Increases in sSC

(A) Timeline. VC was removed by aspiration on P9–P10. Sham incision of skull without lesion served as control (sham). Lesion was confirmed at P13 (Figure S3).

(B) Representative mEPSCs from sham-operated or VC removed animals at P13. Magnified intervals are shown on the right. Dots = supratheshold events.

(C) Model-based analysis (see Figure 1) shows removal of VC inputs before EO causes a 2-fold reduction in the frequency of mEPSCs after EO, compared to sham-operated controls.

(D) Mean amplitude of remaining mEPSCs is larger after cortical removal.

(E) Representative confocal projection through caliber 3 or 4 dendrites after VC lesion or sham surgery.

(F) Quantification of spine and filopodia density 24 hr AEO indicate that VC axons are required for the post-EO filopodia surge on caliber 3 dendrites where cortical inputs dominate (n = 15, *p < 0.05, Student's t test).

increased firing in all layers including L5a (mean increased multiunit spike: 230%, standard deviation [SD] 59%, one-sample t test p = 0.008) and periods of sustained oscillations in the field potential of V1 superficial layers at β-γ frequencies (Figures 8B and 8C). This was surprising, but a similar effect (suppression of rapid oscillations by visual stimuli) has been observed in the cat VC (Kruse and Eckhorn, 1996). The SC did not demonstrate a similar change in network state when the eyes were closed (mean increased multiunit spike rate = 106%, SD 35%, one-sample t test p = 0.7).

To directly test the role of the EC-induced activity state change on visual processing without artifacts from changes in light

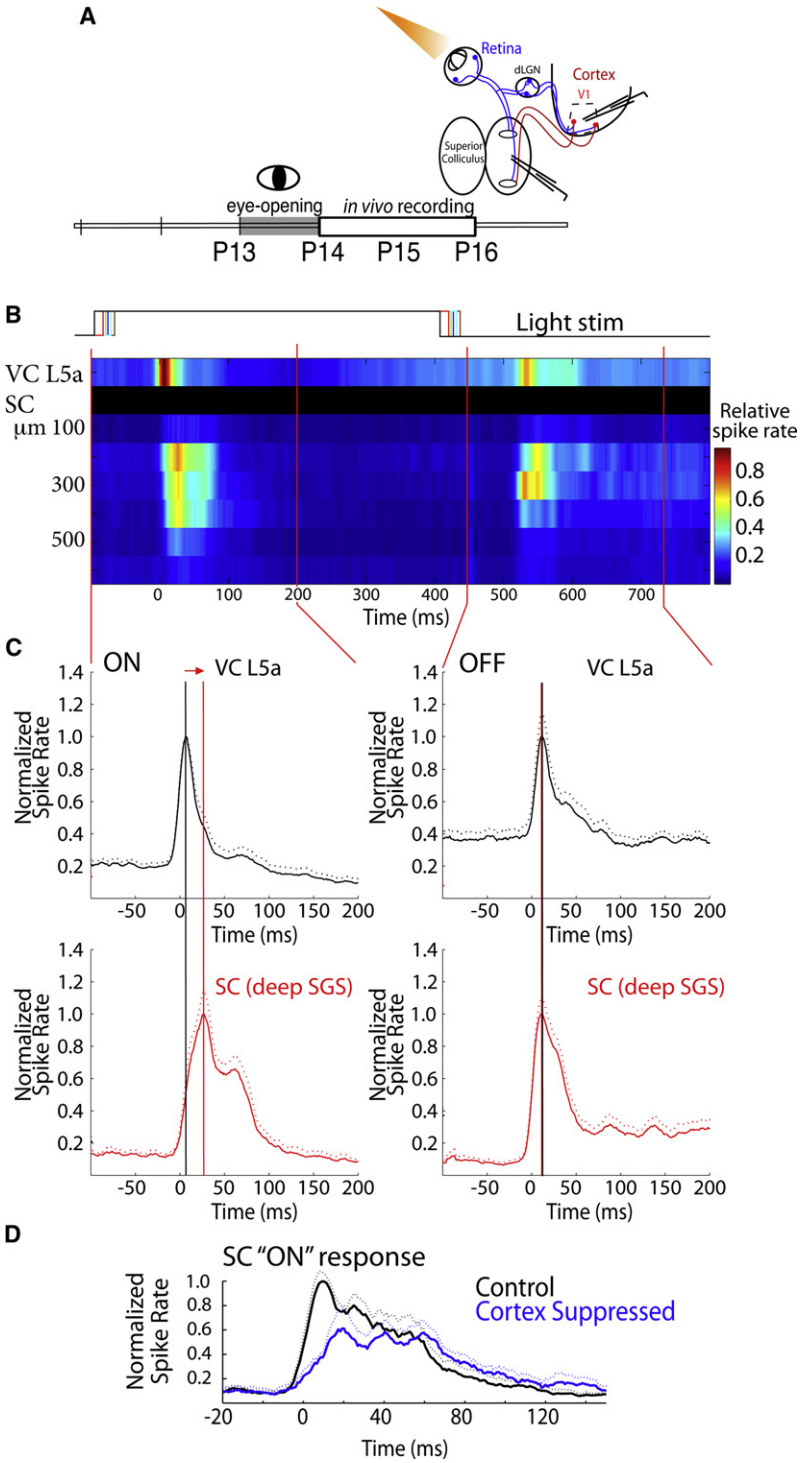

Figure 7. Cortical Visual Responses Precede and Drive Colliculus after EO

(A) Experimental set-up. Simultaneous recording of visual responses 1–2 days after EO in the SC and VC (V1; lower L5a) 1–2 days after EO. Multiunit and field responses to whole field light flash under ambient illumination were collected from awake, unanesthetized rat pups.

(B) Spike rate histograms of mean multiunit spike rate in V1 and throughout the depth of the sSC (n = 100 trials from each of 5 pups). Responses were aligned to the V1 "ON" response in each animal, averaged, and normalized to the maximal spike rate. Visual stimulus timing for each pup is shown above as separate colored line.

(C) Average light-induced spike rates for V1 (L5a) and SC neurons (deep SGS; 200–400 um depth). Graphs show relative differences in timing between L5a and sSC spike rates for ON and OFF responses. Spike rate in each structure was normalized to its maximal rate. Dotted line = SD. Onset of V1 response to light (time = 0) is defined as 40% of the layer 5a peak evoked spike rate. Vertical line = peak response.

(D) Average light-induced spike rates in deep SGS neurons before (Control) or after suppression of V1 cortical activity by spreading depression. No effect on the SC OFF response was detected (not shown). Dotted lines = SD, n = 25 trials from each of 3 pups.

intensity caused by eye-lid manipulation, we identified conditions of visual stimulation that increased the occurrence of this activity state in the eye open condition, namely viewing a nonpatterned stimulus background in low-light conditions. By presenting a light flash while the animal viewed a gray screen stimulus (Figure 8D), we were able to compare the latency between the cortical layer 5a response and the deep SGS response to a whole field light flash of identical intensity when the stimulus was given during an "eye open" or "eye closed" activity state. In eye open trials, the latency of the peak cortical response remained shorter than the peak collicular response by an average delay of ~10 ms (Figure 8E). When stimulation was given in the eye closed state, however, the peak layer 5a response followed, rather than led, the peak collicular response by approximately10 ms (Figure 8F). This shift in relative timing was primarily due to shifts in the cortical layer 5a response, because collicular response latency was not obviously affected, even though the response was diminished by ~40%.

Close examination of the field potential and spiking in individual trials revealed that light evokes a strong, but brief, burst of cortical spikes during the eye open state in both layer 4, and, a short time later, in layer 5a (Figure 8G). In the eye closed state, light induces a shorter initial burst of layer 5a spikes, followed by a second, stronger burst ~10–15 ms later (Figure 8H). Together, the field and spike data suggest that vision through closed eyelids modifies the visual cortical response from a singular visual evoked potential with a single associated peak in firing rate, to a biphasic response resulting from the induction (or phase-resetting) of two phases of ongoing β-γ oscillations. The first phase causes a burst of spikes with similar latency as the normal ON response (though greatly reduced in magnitude). The second,

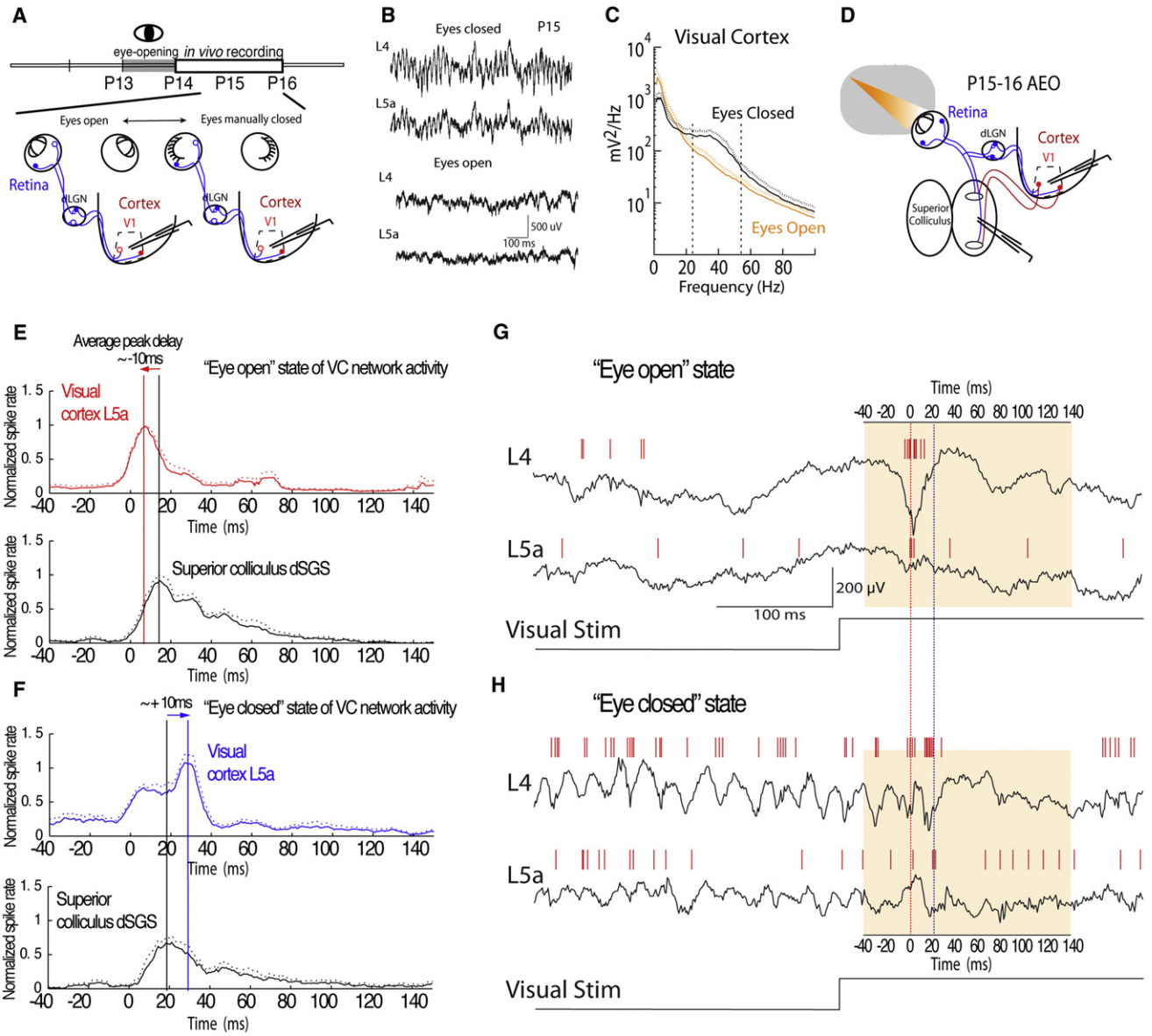

Figure 8. Eye-Closure Induced Changes in Cortical Activity Shift Timing of Peak Corticocollicular Visual Responses

(A) Experimental set-up. To test the effect of eye closure on cortical activity, multielectrode recordings were made throughout the depth of V1 from awake, unanesthetized rats 1–2 days after EO. Both eyelids of each rat were open or manually kept closed during the experiment.

(B) Field potential traces from layer 4 and 5a show prominent rapid oscillations when eyes are closed by the experimenter; these are infrequent when eyes are open.

(C) Frequency power analysis of the layer 4 field potential between the eye open and closed conditions (n = 5 pups). Eye closure was associated with an increase in power in the β-γ range.

(D) Experimental set-up for (E–H). Simultaneous recording from deep SGS and lower L5a 1–2 days after EO in awake rat pups. Visual responses were evoked by whole field light flash while the eyes were open, under conditions where pattern vision was eliminated by a gray screen to increase occurrence of the eye closed activity state. Trials were sorted by the absence or presence of β-γ oscillations indicative of the eye open or eye closed state.

(E) Average multiunit spiking response to ON stimuli in L5a and sSC during the eye open state. Visual cortical output responses precede peak collicular responses by 10 ms. Responses in each structure were normalized to the peak spike rate, and the time-scale is as in Figure 6C.

(F) Average multiunit responses to light onset during the eye closed state. Trials from the eye closed state are associated with a change in the timing of peak L5a responses relative to sSC, causing the majority of light-evoked cortical spikes to follow collicular responses. Responses were normalized to each structure's peak spike rate in the eye open condition (E).

(G) Example of cortical activity during an eye open state. Local field potential (black) with spike locations (red hatch marks) from layers 4 and 5a. Red and blue lines show location of average peak responses in each state. Bottom line shows timing of visual stimulus (flash). Shaded box is time window plotted in (E).

(H) Same animal as in (G) in the eye closed state.

stronger response is observed only in the eye closed state, and yields an abnormally delayed response to light. We propose that this delayed peak response relative to the sSC peak response predisposes corticocollicular inputs to depression, and ultimately a loss of synapses and terminals in the sSC, by a spike-timing mechanism (Kobayashi and Poo, 2004).

DISCUSSION

The initial formation of topographic maps in the sSC occurs before visual experience, relying instead on a combination of chemotrophic cues including Ephrins and Eph kinase gradients, and spontaneous retinal waves. Together these factors align the retinocollicular (Flanagan, 2006; Huberman et al., 2008a) and corticocollicular axon maps (Triplett et al., 2009). This rough corticocollicular topography, however, undergoes extensive refinement and elaboration to form the functional circuit. A number of laboratories, including our own, have found considerable evidence supporting a role for EO and pattern vision in the maturation of visual inputs (Jiang et al., 2010; Lu and Constantine-Paton, 2004; Prusky et al., 2008; Rochefort et al., 2009; Smith and Trachtenberg, 2007; Yoshii et al., 2003). However, few studies have focused on single cell anatomy and function during this initial period when vision starts driving the largely overlapped corticocollicular and retinocollicular visual pathways. Because visuomotor control depends on effective point-to-point convergence of these pathways (Schiller, 2011), we identified and studied an sSC cell type in the deep SGS, DOV neurons, where cortical and retinal axons converge as early as P11. We show in these cells that after the initial alignment of retinal and cortical axons in the sSC, significant synaptic elaboration and refinement of axon terminals is driven by, and critically dependent on, EO. In this subsequent stage, which we call "consolidation," the cortical map becomes functionally integrated with the preestablished retinal map at the level of individual neurons. Our combined electrophysiological and anatomical analysis of collicular and corticocollicular network development 1–2 days after EO suggests that during initial visual experience retinal and cortical axons at visuotopically matched loci cooperate to fire collicular neurons, providing a potential cellular mechanism for cooperation by convergent afferents during initial visual experience (Smith and Trachtenberg, 2007). These data also suggest corticocollicular inputs use a spike-timing mechanism to coinnervate the sSC and probably displace some retinally driven synapses, only when the eyes are open.

Consolidation of the Corticocollicular Input: Role for PSD-95 and Experience

We show, by assaying synaptic density with miniature EPSC recordings from individual DOV neurons, that functional synapses increase rapidly in number and strength after EO. In PSD-95 mutant mice this increase is absent (Figure 1) supporting a requirement for PSD-95, mature NMDARs, and AMPARs in synapse, spine, and probably branch stabilization (Niell et al., 2004; Vickers et al., 2006), as suggested by several studies (reviewed in Xu, 2011).

Removal of ipsilateral VC reduces mEPSC frequency, even when EO occurs on its normal schedule, indicating that the cortical input is normally responsible for increasing synapse number in these cells after EO (Figure 6C). Visual experience guides this process because EO induces a rapid local branching of cortical axon arbors in sSC whereas prevention of EO strips corticocollicular arbors of all but the smallest axon collaterals (Figures 5E and 5F). Eyelid closure is also damaging to existing synapses, causing mEPSC frequency, and spines on cortico-recipient dendrites, to fall to below pre-EO levels (Figures 1D and 5C), a situation reminiscent of the damage to orientation selectivity seen in VC by post-EO lid suture (White et al., 2001).

Strategies for Successful Synaptogenesis Despite Late Arrival of the Corticocollicular Input

We asked how cortical afferents that innervate the colliculus later than retinal afferents can maintain synapses in the sSC, where NMDA-dependent Hebb-like plasticity normally removes low density inputs (Colonnese and Constantine-Paton, 2006; Simon et al., 1992). That they innervate the sSC at all is perplexing, because by virtue of their greater synaptic distance from the retina, cortical action potentials should arrive in sSC long after the direct retinal input has reached the colliculus. Such assumptions suggest a reduced ability of cortical inputs to fire sSC cells, which should lead to depression of corticocollicular inputs.

The present data suggest several ways that the brain solves this problem. First, even before EO, cortical axons target regions of DOV cell bodies proximal to the spike initiating zone (Figure 3) and later concentrate on proximal dendrites where they are located in adulthood (Figure 2). This is expected to maximize their depolarization of DOV neurons, which have axons originating ventrally from the soma (Bekkers and Stevens, 1996; Spruston, 2008). Indeed, we found cortex to be an effective driver of collicular neuronal spiking as early as 1 day after EO in the deep SGS where DOV neurons are located. Targeting of proximal locations may be a strategy that is widely used in the developing CNS to aid synaptogenesis (Hashimoto et al., 2009).

How proximal regions are targeted is uncertain. Some data suggest a laminar selectivity by genetically specified retinal ganglion cell axons within the sSC (Huberman et al., 2008b; Siegert et al., 2009), and DOV neurons sit at the level of cortical axon ingrowth, but this does not prove that the laminar ingrowth or target neurons are prespecified. Because VC axons initially support fewer synapses compared to the preestablished retinal projection, this could render them more powerful competitors for the previously retina occupied dendritic sites (Figure 3). Support for such a mechanism has been obtained during elimination of competing motor neuron axons on young muscle fibers (Kasthuri and Lichtman, 2003).

Our data suggests a second reason why later arising VC synapses can form stable sSC contacts. Specifically, during pattern vision after EO, we find a rapid flow of excitation through the thalamocortical pathway. Despite a direct retinal input to sSC, peak cortical spiking in L5a precedes the collicular response (Figures 7 and 8). Thus, the ability of cortical neurons to drive collicular neurons with a short (<10 ms) latency could facilitate cortical synapse stabilization through a spike timing dependent mechanism (Froemke et al., 2005; Kobayashi and Poo, 2004; Zhang et al., 1998).

The decreased and sluggish drive of SC units we observed after cortical suppression is somewhat at odds with recent single unit observations in anesthetized adult rodents (Wang et al., 2010). Differences in age and anesthesia will surely contribute to the observed differences, particularly in light of the delayed development of inhibition in the SC (Shi et al., 1997). We do know that anesthesia can significantly modify both spontaneous and visually evoked activity in the rat (Colonnese and Khazipov, 2010; Colonnese et al., 2010), and it is reasonable to assume that age, anesthesia, and/or the fact that responses in Wang et al. (2010) included both superficial and deep SGS could account for this.

That the cortical timing advantage after eye opening is reversed during eye closure by the changes in the activity state of VC is interesting given the pruning of corticocollicular terminals and loss of collicular inputs with prolonged EC. This timing reversal involves induction of rapid oscillations in the superficial cortical layers and increased spiking in all layers, which was not observed in sSC. This modulation of cortical state can potentially explain the regressive effects of eye closure on corticocollicular axons by two mechanisms. First, the increased firing of corticocollicular neurons in the eye closed state without a concomitant increase in firing of their collicular partners will result in persistent presynaptic activity without correlated postsynaptic firing, leading to long-term depression (Hata et al., 1999). Second, the eye closed cortical state change modulates the timing of light-induced corticocollicular activity, causing the majority of cortical spikes to follow collicular light responses by approximately 10 ms, within the spike timing window for depression. The initial early response does not disappear, but is greatly reduced compared to the delayed response (Figure 8F). One must conclude that some potentiation of corticocollicular synapses could continue to occur during eye closure, but that the balance is tipped in favor of depression. Further experiments will be necessary to determine the generative mechanism of these immature oscillations and which of these strategies is the more relevant to the experience-dependent consolidation of cortical and retinal inputs in the developing animal.

Conclusions

Taking advantage of the thy-1 eGFP-S mouse that, early in development, fills DOV neurons in the cortico- and retino-recipient sSC with GFP, we show that the ability of the late-arriving cortical input to successfully coinnervate this one common sSC neuron type depends on vision and the activity state of the cortical network, and is probably aided by targeting to powerful proximal dendritic and somatic domains. When pattern vision is prevented the consolidation of these inputs is eliminated; corticocollicular axon arbors and many spines on cortico-recipient dendrites essentially disappear. Our data indicate elimination of V1 connections to its targets could result from dark rearing, eye closure, or other disruptions of early pattern vision, and suggest a powerful role for modulation of cortical network activity in experience-dependent plasticity. These data also provide a rodent model for investigations into recovery from early sensory deprivation that may have specific implications for the potential recovery of human vision after late cataract removal or trauma to the early visual pathway. The rapid experience-dependent interaction between two mapped afferents that we describe may contribute to the process that rapidly restores some sensory capabilities such as cross-modal mapping after successful cataract removal (Held et al., 2011).

EXPERIMENTAL PROCEDURES

Animals

Procedures followed MIT IACUC-approved protocols. Mice were wild-type C57BL/6 background (Jackson Laboratories), homozygous PSD-95 mutants (Migaud et al., 1998) gifted by M. Wilson with consent of S.G. Grant, or Thy-1 eGFP-S transgenics gifted by E. Nedivi with consent of G. Feng (Feng et al., 2000). Dams were checked twice a day for litters and the day of birth was "P0." Natural EO in this strain began as early as P11, and was complete by P14. EO was controlled in mice using a thin layer of glue (Vetbond, 3M), and in Sprague-Dawley rats (Taconic) with sutures (Ethicon) and glue. Fixation and histology were as described (Colonnese et al., 2005) (Supplemental Experimental Procedures).

Confocal Microscopy

Serial sections from each Thy1-eGFP animal were scanned under epifluorescence (Nikon 20×/0.75 NA objective) for well-labeled DOV neurons. In eGFP mice axons could be observed originating from the basal portion of the soma and followed ventrally directly toward the deeper layers of SC. These cells are most consistent with the "cylindrical neurons with dorsoventrally oriented dendrites" within category Type 5b as described (Tokunaga and Otani (1976). Each cell with a majority (>80%–90%) of its dendritic arbor well labeled and present in a single slice was selected for further analysis. Beginning at the soma, confocal z series of portions of the dendritic arbor were collected at high magnification with a 60×/1.4 NA oil-immersion objective and 2× digital zoom at 0.5 μm intervals in the z axis on a Nikon PCM2000 (MVI) with a pinhole size of 23 μm using SimplePCI acquisition software (Compix), for a final pixel resolution of 0.1 μm × 0.1 μm (*xy*) and ~0.03 μm^2 out of plane. The acquisition gain was determined independently for each cell to be below the maximum threshold that caused saturation of pixels in spines. Finally, lower-magnification image(s) of each cell (60×/1.4 NA, 0.2 μm × 0.2 μm *xy* at 2 μm intervals) were collected for later reconstruction of the location of each dendrite on the cell's arbor. In some figures, confocal projections were contrast enhanced and a median Gaussian filter (1–2 pixels) applied. Z series were exported to Softworx for SGI (DeltaVision) for spine and filopodia analysis (Supplemental Experimental Procedures).

Anterograde Afferent Labeling

Retinal and cortical afferents to the SGS were labeled by injection of 0.5% Alexa 488-, 555-, or 647-conjugated Cholera Toxin B subunits (Invitrogen) in 2% DMSO/sterile PBS pH 7.4 using a glass micropipette (CellTram Vario, Eppendorf). Retinal injection was intravitreal. To label cortex, 1–3 μl of dye solution was injected through a small burr hole in medio-posterior cortex (Using Paxinos' coordinates from λ: 3 mm in adult mice, scaled for other ages). After 1–3 days, animals were perfused, and successful injections confirmed by fluorescent stereomicroscopy.

Axodendritic Proximity Assay

Confocal image stacks were examined for colocalization between eGFP-labeled neurons and anterogradely labeled retinal and cortical axons using ImageJ (NIH). Only pixels exceeding a fixed intensity threshold were used to identify colocalization. This threshold was empirically determined by evaluation of the threshold required to discriminate in-focus from out-of-focus fluorescence, and was set at 5.5 SD above the mean pixel intensity. Confocal z series encompassing the neuron were batch processed for colocalized pixels using an automated ImageJ algorithm. The density and localization of the overlapped pixels on dendritic branches of individual neurons was measured in Softworx, using the original neuronal image stack overlapped with a binary image stack of the colocalized pixels (Supplemental Experimental Procedures).

Cortical Axon Analysis

Small Gelfoam threads (Pharmacia) were soaked in saturated $DiIC_{18}$ (Molecular Probes, Invitrogen) in dimethylformamide (DMF) and dried overnight. Individual strands were inserted in V1 under the pia. Two to three days later, confocal images were collected throughout the depth of each parasagittal section and the A-P axis with a 40×/1.30 NA oil-immersion objective (Nikon) or a 20×/0.75 NA air lens (1.5 μm z step). Blind, 3D single-arbor reconstructions of the portion of the axon contained in each section was done in Neurolucida (MicroBrightField) by creating a high resolution montage of the entire A-P axis. Discrete cortical axons were traced caudally from the brachium of the sSC. Branches that exited the slice were marked and terminals with major branches leaving the section were discarded. For quantitative analysis, a 40 μm ×40 μm grid overlay was placed over 100 μm-deep image stacks, yielding 160 mm^3 volumes of tissue for analysis of labeled processes in every fourth volume along the A-P axis using Neurolucida.

Whole Cell Electrophysiology

Whole-cell recordings were from the deep SGS of C57BL/6 mouse SC in acute parasagittal slices as described (Lu and Constantine-Paton, 2004) following Hestrin (1992) (see Supplemental Experimental Procedures for details). Recorded neurons were selected under IR-DIC based on their position in the intermediate portion of the SGS, with vertically oriented or pear-shaped somas and dorsally oriented, vertical proximal dendrites. These criteria correctly identified DOV neurons as confirmed by inclusion of Alexa 488 hydrazide (Invitrogen) in the intracellular solution. Cortical lesion experiments were conducted on a different electrophysiology set-up than other experiments. To avoid bias, sham experiments were conducted on littermates using the same equipment, and the lesion group was statistically compared only to sham-operated animals. Event data was exported to MATLAB for model-based analysis (Supplemental Experimental Procedures).

In Vivo Electrophysiology

Procedures for recording were previously described (Colonnese et al., 2010) (see Supplemental Experimental Procedures for details). Experiments were conducted in accordance with the Animal Care and Use Committee guidelines (INSERM, France). Eyes were kept closed by applying clear tape to a thin layer of glue. EO was verified by eye. Waking state was verified by tonic EMG activity. Visual stimulation details are provided in the text and Supplemental Experimental Procedures. Simultaneous VC and sSC recordings used pulled glass microelectrodes (1–2 MΩ) coupled to a direct-current amplifier (Axon Instruments) and multisite linear array silicon Michigan Probes (Neuronexus Tech) coupled to a custom built AC amplifier (1000×, bandpass 1 Hz–5 kHz). V1 recordings were localized at 3.0–3.2 mm lateral to midline, and 0.0–0.5 rostral to λ, and sSC recordings to 0.5–0.8 lateral, 1 mm rostral. Cortical layer identification was accomplished via multiple criteria. Anatomical sections show layer 4 to be located 400–500 μm below the pial surface. Layer 4 was identified by the peak visual response (Colonnese et al., 2010). The collicular projecting layer (lower 5a) was defined as 200 μm below L4 and containing large, spontaneously active units (Le Bon-Jego and Yuste, 2007). Multiunit firing was identified by high-pass filtering above 300 Hz and simple threshold discrimination (more than 4.3 times SD of baseline noise). Good discrimination was verified for each channel.

SUPPLEMENTAL INFORMATION

Supplemental Information includes Supplemental Experimental Procedures and five figures and can be found with this article online at doi:10.1016/j.neuron.2011.06.023.

ACKNOWLEDGMENTS

We would like to thank R. Desimone for helpful comments, C. Yee and A. Birdsey-Benton for technical assistance, W. Lee for transferring mutant mice, and C. Tunca for biochemistry advice. This work was supported by NIH grant EY006039 to M.C.-P. M.T.C. was supported by a grant to Rustem Khazipov (INSERM, France) from the Agence Nationale de Recherche, France.

Accepted: June 16, 2011
Published: August 24, 2011

REFERENCES

Bakkum, B.W., Benevento, L.A., and Cohen, R.S. (1991). Effects of light/dark- and dark-rearing on synaptic morphology in the superior colliculus and visual cortex of the postnatal and adult rat. J. Neurosci. Res. *28*, 65–80.

Béïque, J.C., and Andrade, R. (2003). PSD-95 regulates synaptic transmission and plasticity in rat cerebral cortex. J. Physiol. *546*, 859–867.

Bekkers, J.M., and Stevens, C.F. (1996). Cable properties of cultured hippocampal neurons determined from sucrose-evoked miniature EPSCs. J. Neurophysiol. *75*, 1250–1255.

Chen, C., and Regehr, W.G. (2000). Developmental remodeling of the retinogeniculate synapse. Neuron *28*, 955–966.

Colonnese, M.T., and Constantine-Paton, M. (2001). Chronic NMDA receptor blockade from birth increases the sprouting capacity of ipsilateral retinocollicular axons without disrupting their early segregation. J. Neurosci. *21*, 1557–1568.

Colonnese, M.T., and Constantine-Paton, M. (2006). Developmental period for N-methyl-D-aspartate (NMDA) receptor-dependent synapse elimination correlated with visuotopic map refinement. J. Comp. Neurol. *494*, 738–751.

Colonnese, M.T., and Khazipov, R. (2010). "Slow activity transients" in infant rat visual cortex: a spreading synchronous oscillation patterned by retinal waves. J. Neurosci. *30*, 4325–4337.

Colonnese, M.T., Kaminska, A., Minlebaev, M., Milh, M., Bloem, B., Lescure, S., Moriette, G., Chiron, C., Ben-Ari, Y., and Khazipov, R. (2010). A conserved switch in sensory processing prepares developing neocortex for vision. Neuron *67*, 480–498.

Colonnese, M.T., Zhao, J.P., and Constantine-Paton, M. (2005). NMDA receptor currents suppress synapse formation on sprouting axons in vivo. J. Neurosci. *25*, 1291–1303.

Constantine-Paton, M., Cline, H.T., and Debski, E. (1990). Patterned activity, synaptic convergence, and the NMDA receptor in developing visual pathways. Annu. Rev. Neurosci. *13*, 129–154.

Dhande, O.S., Hua, E.W., Guh, E., Yeh, J., Bhatt, S., Zhang, Y., Ruthazer, E.S., Feller, M.B., and Crair, M.C. (2011). Development of single retinofugal axon arbors in normal and β2 knock-out mice. J. Neurosci. *31*, 3384–3399.

Feng, G., Mellor, R.H., Bernstein, M., Keller-Peck, C., Nguyen, Q.T., Wallace, M., Nerbonne, J.M., Lichtman, J.W., and Sanes, J.R. (2000). Imaging neuronal subsets in transgenic mice expressing multiple spectral variants of GFP. Neuron *28*, 41–51.

Flanagan, J.G. (2006). Neural map specification by gradients. Curr. Opin. Neurobiol. *16*, 59–66.

Froemke, R.C., Poo, M.M., and Dan, Y. (2005). Spike-timing-dependent synaptic plasticity depends on dendritic location. Nature *434*, 221–225.

Hashimoto, K., Ichikawa, R., Kitamura, K., Watanabe, M., and Kano, M. (2009). Translocation of a "winner" climbing fiber to the Purkinje cell dendrite and subsequent elimination of "losers" from the soma in developing cerebellum. Neuron *63*, 106–118.

Hata, Y., Tsumoto, T., and Stryker, M.P. (1999). Selective pruning of more active afferents when cat visual cortex is pharmacologically inhibited. Neuron *22*, 375–381.

Held, R., Ostrovsky, Y., de Gelder, B., Gandhi, T., Ganesh, S., Mathur, U., and Sinha, P. (2011). The newly sighted fail to match seen with felt. Nat. Neurosci. *14*, 551–553.

Hestrin, S. (1992). Developmental regulation of NMDA receptor-mediated synaptic currents at a central synapse. Nature *357*, 686–689.

Huberman, A.D., Feller, M.B., and Chapman, B. (2008a). Mechanisms underlying development of visual maps and receptive fields. Annu. Rev. Neurosci. *31*, 479–509.

Huberman, A.D., Manu, M., Koch, S.M., Susman, M.W., Lutz, A.B., Ullian, E.M., Baccus, S.A., and Barres, B.A. (2008b). Architecture and

activity-mediated refinement of axonal projections from a mosaic of genetically identified retinal ganglion cells. Neuron *59*, 425–438.

Inoue, K., Terashima, T., and Inoue, Y. (1992). Postnatal development of the corticotectal projection from the visual cortex of the mouse. Okajimas Folia Anat. Jpn. *68*, 319–331.

Jiang, B., Huang, S., de Pasquale, R., Millman, D., Song, L., Lee, H.K., Tsumoto, T., and Kirkwood, A. (2010). The maturation of GABAergic transmission in visual cortex requires endocannabinoid-mediated LTD of inhibitory inputs during a critical period. Neuron *66*, 248–259.

Kasthuri, N., and Lichtman, J.W. (2003). The role of neuronal identity in synaptic competition. Nature *424*, 426–430.

Khachab, M.Y., and Bruce, L.L. (1999). The development of corticocollicular projections in anophthalmic mice. Brain Res. Dev. Brain Res. *114*, 179–192.

Kobayashi, K., and Poo, M.M. (2004). Spike train timing-dependent associative modification of hippocampal CA3 recurrent synapses by mossy fibers. Neuron *41*, 445–454.

Krug, K., Akerman, C.J., and Thompson, I.D. (2001). Responses of neurons in neonatal cortex and thalamus to patterned visual stimulation through the naturally closed lids. J. Neurophysiol. *85*, 1436–1443.

Kruse, W., and Eckhorn, R. (1996). Inhibition of sustained gamma oscillations (35-80 Hz) by fast transient responses in cat visual cortex. Proc. Natl. Acad. Sci. USA *93*, 6112–6117.

Le Bon-Jego, M., and Yuste, R. (2007). Persistently active, pacemaker-like neurons in neocortex. Front Neurosci. *1*, 123–129.

Lu, W., and Constantine-Paton, M. (2004). Eye opening rapidly induces synaptic potentiation and refinement. Neuron *43*, 237–249.

Lund, R.D., and Lund, J.S. (1971). Synaptic adjustment after deafferentation of the superior colliculus of the rat. Science *171*, 804–807.

Maffei, A., Nelson, S.B., and Turrigiano, G.G. (2004). Selective reconfiguration of layer 4 visual cortical circuitry by visual deprivation. Nat. Neurosci. *7*, 1353–1359.

Magee, J.C., and Cook, E.P. (2000). Somatic EPSP amplitude is independent of synapse location in hippocampal pyramidal neurons. Nat. Neurosci. *3*, 895–903.

Maurer, D., Lewis, T.L., and Mondloch, C.J. (2005). Missing sights: consequences for visual cognitive development. Trends Cogn. Sci. (Regul. Ed.) *9*, 144–151.

Migaud, M., Charlesworth, P., Dempster, M., Webster, L.C., Watabe, A.M., Makhinson, M., He, Y., Ramsay, M.F., Morris, R.G., Morrison, J.H., et al. (1998). Enhanced long-term potentiation and impaired learning in mice with mutant postsynaptic density-95 protein. Nature *396*, 433–439.

Niell, C.M., Meyer, M.P., and Smith, S.J. (2004). In vivo imaging of synapse formation on a growing dendritic arbor. Nat. Neurosci. *7*, 254–260.

Ostrovsky, Y., Andalman, A., and Sinha, P. (2006). Vision following extended congenital blindness. Psychol. Sci. *17*, 1009–1014.

Philpot, B.D., Sekhar, A.K., Shouval, H.Z., and Bear, M.F. (2001). Visual experience and deprivation bidirectionally modify the composition and function of NMDA receptors in visual cortex. Neuron *29*, 157–169.

Prusky, G.T., Silver, B.D., Tschetter, W.W., Alam, N.M., and Douglas, R.M. (2008). Experience-dependent plasticity from eye opening enables lasting, visual cortex-dependent enhancement of motion vision. J. Neurosci. *28*, 9817–9827.

Rochefort, N.L., Garaschuk, O., Milos, R.I., Narushima, M., Marandi, N., Pichler, B., Kovalchuk, Y., and Konnerth, A. (2009). Sparsification of neuronal activity in the visual cortex at eye-opening. Proc. Natl. Acad. Sci. USA *106*, 15049–15054.

Schiller, P.H. (2011). The superior colliculus and visual function. Compr. Physiol. (*Suppl*), 457–505.

Shi, J., Aamodt, S.M., and Constantine-Paton, M. (1997). Temporal correlations between functional and molecular changes in NMDA receptors and GABA neurotransmission in the superior colliculus. J. Neurosci. *17*, 6264–6276.

Siegert, S., Scherf, B.G., Del Punta, K., Didkovsky, N., Heintz, N., and Roska, B. (2009). Genetic address book for retinal cell types. Nat. Neurosci. *12*, 1197–1204.

Simon, D.K., and O'Leary, D.D. (1992). Development of topographic order in the mammalian retinocollicular projection. J. Neurosci. *12*, 1212–1232.

Simon, D.K., Prusky, G.T., O'Leary, D.D., and Constantine-Paton, M. (1992). N-methyl-D-aspartate receptor antagonists disrupt the formation of a mammalian neural map. Proc. Natl. Acad. Sci. USA *89*, 10593–10597.

Smith, S.L., and Trachtenberg, J.T. (2007). Experience-dependent binocular competition in the visual cortex begins at eye opening. Nat. Neurosci. *10*, 370–375.

Smith, M.A., Ellis-Davies, G.C., and Magee, J.C. (2003). Mechanism of the distance-dependent scaling of Schaffer collateral synapses in rat CA1 pyramidal neurons. J. Physiol. *548*, 245–258.

Spruston, N. (2008). Pyramidal neurons: dendritic structure and synaptic integration. Nat. Rev. Neurosci. *9*, 206–221.

Thong, I.G., and Dreher, B. (1986). The development of the corticotectal pathway in the albino rat. Brain Res. *390*, 227–238.

Tokunaga, A., and Otani, K. (1976). Dendritic patterns of neurons in the rat superior colliculus. Exp. Neurol. *52*, 189–205.

Triplett, J.W., Owens, M.T., Yamada, J., Lemke, G., Cang, J., Stryker, M.P., and Feldheim, D.A. (2009). Retinal input instructs alignment of visual topographic maps. Cell *139*, 175–185.

Vickers, C.A., Stephens, B., Bowen, J., Arbuthnott, G.W., Grant, S.G., and Ingham, C.A. (2006). Neurone specific regulation of dendritic spines in vivo by post synaptic density 95 protein (PSD-95). Brain Res. *1090*, 89–98.

Warton, S.S., and McCart, R. (1989). Synaptogenesis in the stratum griseum superficiale of the rat superior colliculus. Synapse *3*, 136–148.

Wang, L., Sarnaik, R., Rangarajan, K., Liu, X., and Cang, J. (2010). Visual receptive field properties of neurons in the superficial superior colliculus of the mouse. J. Neurosci. *30*, 16573–16584.

White, L.E., Coppola, D.M., and Fitzpatrick, D. (2001). The contribution of sensory experience to the maturation of orientation selectivity in ferret visual cortex. Nature *411*, 1049–1052.

Xu, W. (2011). PSD-95-like membrane associated guanylate kinases (PSD-MAGUKs) and synaptic plasticity. Curr. Opin. Neurobiol. *21*, 306–312.

Yoshii, A., Sheng, M.H., and Constantine-Paton, M. (2003). Eye opening induces a rapid dendritic localization of PSD-95 in central visual neurons. Proc. Natl. Acad. Sci. USA *100*, 1334–1339.

Yu, L., Rowland, B.A., and Stein, B.E. (2010). Initiating the development of multisensory integration by manipulating sensory experience. J. Neurosci. *30*, 4904–4913.

Zhang, L.I., Tao, H.W., Holt, C.E., Harris, W.A., and Poo, M. (1998). A critical window for cooperation and competition among developing retinotectal synapses. Nature *395*, 37–44.